Channel profiles around Himalayan river anticlines: Constraints on their formation from digital elevation model analysis

Jörg Robl,[1] Kurt Stüwe,[1] and Stefan Hergarten[1]

Received 2 October 2007; revised 25 January 2008; accepted 6 March 2008; published 20 June 2008.

[1] We present a comparison between measured and numerically modeled channel profiles of rivers in two important drainage basins of Central Nepal: the Kali-Gandaki and the Arun drainage basins. Modeled channel profiles are based on a simple stream power approach using best fit exponents defining the nonlinearities in the relative contributions of local channel gradient and water flux to erosion rate. Our analysis of the stream power in the whole river network confirms the work of other authors that a 50- to 80-km-wide zone, roughly corresponding to the High Himalayan topography, is subjected to rapid rock uplift. We suggest a model where the uplift of this zone is driven by erosion and isostatic response, so that centers of maximum uplift are located within the main channels of the north–south draining rivers. We also suggest that the rate of uplift slows down with increasing distance to the main channels. Such a spatial distribution of the uplift leads ultimately to the formation of river anticlines as observed along all major Himalayan rivers. We propose that the formation of river anticlines along south draining Himalayan rivers was accelerated by a sudden increase of the drainage area and discharge when the rivers captured orogen-parallel drainages on the north side of the range. This may follow successive headward cutting into the Tibetan Plateau. The model is confirmed by differences between main channels and east–west running tributaries. Time-dependent numerical models predict that capture events cause strongly elevated erosion rates in the main channel.
Citation: Robl, J., K. Stüwe, and S. Hergarten (2008), Channel profiles around Himalayan river anticlines: Constraints on their formation from digital elevation model analysis, *Tectonics*, *27*, TC3010, doi:10.1029/2007TC002215.

1. Introduction

[2] The India-Asian collision zone undoubtedly represents the most impressive orogen on Earth, hosting the world's highest peaks and greatest elevated plateau. Interestingly, many of the huge drainage systems developed around this orogen originate within the Tibetan Plateau north of the highest peaks of the Himalayas and drain southward, perpendicular to the strike of the orogen toward the Indian Ocean (Figure 1). As such, the Himalaya is the only major mountain belt on Earth that features no drainage divide. This geometry has given rise to an active discussion on the nature of this first-order morphological geometry. In particular, there is an active debate if the drainages cause deformation along the topographic front of the range or if the river geometry is the consequence of deformation. In other words, is the morphology of the orogen controlled by erosion or tectonics [*Thiede et al.*, 2005]?

[3] Recent studies of uplift and erosion along some of the major south draining Himalayan rivers could show that the current morphology is most likely reflecting a feedback between active tectonics, climate and erosion [e.g., *Thiede et al.*, 2004; *Wobus et al.*, 2003; *Grujic et al.*, 2006], and is not inherited from past tectonics (Pliocene reactivation of the MCT) [e.g., *Harrison et al.*, 1997]. This is based on identifying an about 50 km wide orogen parallel zone at the front of the High Himalayan Range that is characterized by very rapid erosion- and high uplift rates [e.g., *Seeber and Gornitz*, 1983; *Lavé and Avouac*, 2001] and young cooling ages [*Wobus et al.*, 2006a]. However, the complex feedbacks that control uplift and erosion in this region are still under debate. Early studies explained the rise of the highest peaks by a simple model in which the incision of large valleys is isostatically compensated by localized uplift [*England and Molnar*, 1990; *Montgomery*, 1994]. More recently some authors have argued that the high erosion rates caused active thrusting at the front of the high range [e.g., *Wobus et al.*, 2005] following the model of channel flow extrusion [*Beaumont et al.*, 2004]. Others have proposed for a midcrustal ramp along the Main Himalayan Thrust [e.g., *Lavé and Avouac*, 2001] or the growth of a midcrustal duplex [e.g., *Bollinger et al.*, 2006].

[4] One feature that may help to constrain this debate is the Himalayan river anticlines [*Oberlander*, 1985]. These anticlines are a major updoming of shallow structures in the areas of the major valleys. *Montgomery and Stolar* [2006] suggested that these anticlines do indeed form in response to the incision of the major drainages implying that the west–east striking about 50-km-wide zone of rock uplift identified by studies mentioned above, should change in uplift rate along strike. Modeling studies have compared the stream power of the major drainages to constrain the north–south extent of the uplifting zone to about 50 km, but have not attempted to investigate along strike variations in uplift rate that would confirm the causes of formation of the river

[1]Department for Earth Sciences, University of Graz, Graz, Austria.

0278-7407/08/2007TC002215$12.00

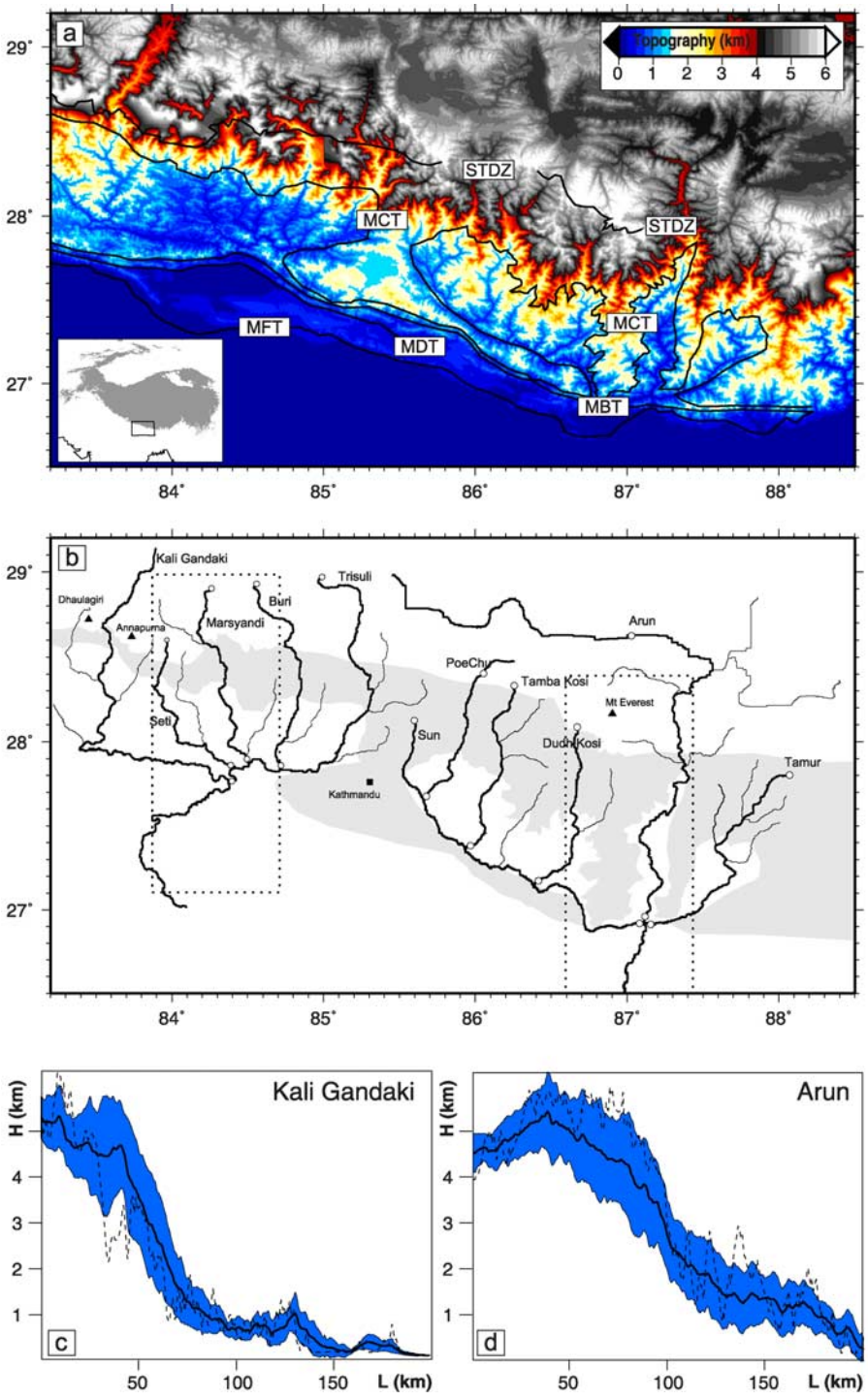

Figure 1. (a) Topographic map of the drainage systems investigated. The gray shaded region in the inset is characterized by a surface elevation above 3000 m. The principal structures in the region are: Main Frontal Thrust, MFT; Main Dun Thrust, MDT; Main Boundary Thrust, MBT; Main Central Thrust, MCT; and South Tibetan Detachment Zone, STDZ. (b) Same area as in Figure 1a showing major rivers in the Kali-Gandaki (in the west) and Arun (in the east) drainage basins. The gray shaded area is the central Himalayan Crystalline Complex between MCT and STDZ. The two punctuated boxes indicate the position of the swath profiles shown in Figures 1c and 1d. The small dots on the rivers correspond to the starting and end points of the channel profiles shown on Figure 3. The solid and dashed lines in Figures 1c and 1d stand for the mean surface elevation and the surface elevation along a centered profile line along the swath profile, respectively. The blue shaded area indicates the standard deviation.

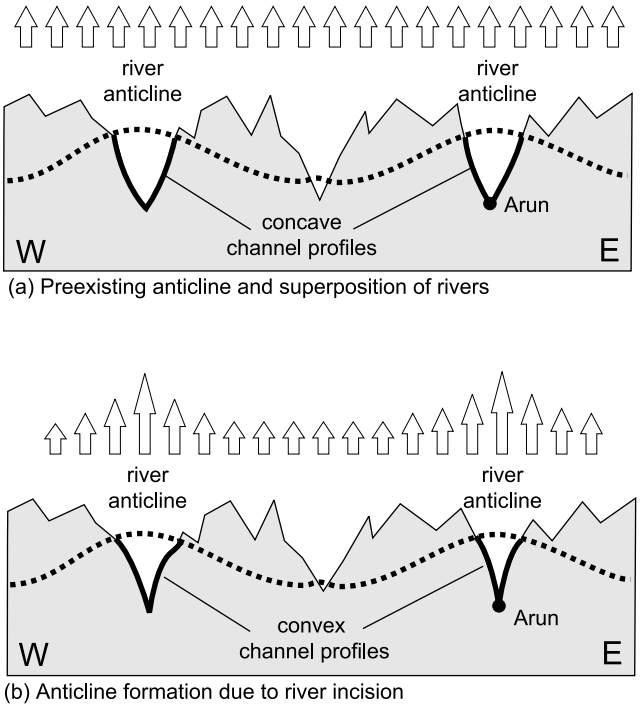

Figure 2. Cartoon illustrating different models for the formation of river anticlines and their predictions for channel profiles of subsidiary drainages running into the major south draining Himalayan rivers. The dotted line shows a formerly planar marker that was folded by the formation of anticlines. Uplift is indicated by the length of the arrows. (a) Preexisting anticline and superposition of rivers. (b) Anticline formation due to river incision.

anticlines and constrain erosion as the driving force of deformation.

[5] In this paper we present further information on this debate by comparing channel profiles of selected drainages with numerically modeled channel profiles and with numerical estimates of stream power in their drainage basins. We interpret departures between model and observations in terms of their tectonic causes in both north–south running main channels and east–west running tributaries. We have selected the Arun and the Kali-Gandaki drainage systems for our analysis, first because there is an abundant body of literature on these rivers including several modeling studies with similar approaches [e.g., *Wobus et al.*, 2006a] and second because they include several major rivers with significant river anticlines (e.g., Arun) (Figure 1). We will show that the river anticlines are likely to be a young feature driven by drainage incision and correlate their formation age with the break through and capture of selected rivers into the Tibetan region. We illustrate our discussion with some simple numerical model experiments that predict the rates of head-ward cutting of south draining rivers as a possible mechanism for capturing of orogen parallel draining rivers within the Tibetan Plateau.

[6] The nature of uplift within the about 50 km wide zone at the front of the Himalayan range should be reflected in differences between channel profiles of rivers that drain parallel versus perpendicular to this zone. If the uplift were tectonically driven [e.g., *Harrison et al.*, 1997; *Catlos et al.*, 2001], we would expect rather constant uplift rates in strike of this zone. This would also mean that the observed anticlines were preexisting and the rivers are superposed (Figure 2a). Tributaries that flow into the main channels within this zone should have concave channel profiles and constant stream power. The main channels should be characterized by knickpoints at northern and southern border of the uplifting zone and by constant but elevated stream power within the zone. In contrast, if the uplift of this zone is controlled by river incision and isostatic response and a feedback between those [e.g., *Thiede et al.*, 2004; *Vannay et al.*, 2004], the loci of maximum uplift should be centered at the main channels (Figure 2b). The rate of uplift should decrease with increasing distance from the main channel. In this case, the formation of anticlines is related to river incision and therefore a young feature. Main channels activating the uplift are far from equilibrium and therefore characterized by highly disturbed channel profiles. Tributaries within this corridor should be featured by convex channel profiles and increasing stream power from the spring to the confluence point with the main channel.

2. Tectonic and Geomorphological Setting

[7] The Tibetan Plateau and Himalaya, including the highest peaks of the world, evolved during 50 ma of convergence between the Indian and Eurasian plate [e.g., *Yin and Harrison*, 2000]. Since the onset of the Indo-Asian collision, an average convergence rate of about 5 cm a^{-1} caused at least 1.400 km of north–south shortening in the orogen [*Patriat and Achache*, 1984; *Larson et al.*, 1999; *Yin and Harrison*, 2000]. During collision, the Indian plate was subducted underneath the Asian plate causing crustal thickening in the orogen, uplift of the Himalayan Range and east-directed lateral escape [*Tapponier and Molnar*, 1977; *Avouac and Tapponier*, 1993].

[8] The diachronous uplift of the Tibetan Plateau is not directly related to indentation of the Indian plate into Asia and the mechanism for the uplift of the Tibetan Plateau is still under debate (e.g., delamination of the mantle lithosphere [*England and Houseman*, 1989; *Molnar et al.*, 1993; *Chung et al.*, 1998] (see also K. Stüwe et al., Modeling the influence of horizontal advection, deformation and late uplift on drainage development in the India-Asia collision zone, submitted to *Tectonics*, 2008) (hereinafter Stüwe et al., submitted manuscript, 2008). However, no matter what exactly was the timing for the uplift at various regions of the Tibetan Plateau, observations on the southern slope of the Himalayan range show that the evolution of the Himalayan thrust belt started in the Eocene [e.g., *Robinson et al.*, 2003]. The main tectonostratigraphic units of the Himalayan belt (Tibetan Himalaya, Greater Himalaya, Lesser Himalaya, Sub Himalaya) are separated by major fault systems [*Gansser*, 1964] (Figure 1a). Form north to south these are the South Tibetan Detachment Zone (STDZ), the Main Central Thrust (MCT) and the Main Boundary Thrust

Table 1. Characteristics of Rivers and Subbasins of the Kali-Gandaki and the Arun Drainage System

River Name	Spring (Longitude, Latitude, Elevation)	Confluence (Longitude, Latitude, Elevation)	Drainage Area (km^2)	Channel Length (km)	Confluence
		Kali-Marsyandi Drainage System			
Complete Basin	-	83.96°E, 27.50°N	36,118		K+S+M+B+T
Kali	83.97°E, 29.31°N, 4588 m	84.42°E, 27.74°N, 189 m	11,728	382	S+M+B+T
Seti	84.02°E, 28.58°N, 5931 m	84.46°E, 27.82°N, 303 m	2987	144	M+B+T
Marsyandi	84.31°E, 28.87°N, 5860 m	84.56°E, 27.85°N, 372 m	4781	165	B+T
Buri	84.60°E, 28.92°N, 5381 m	84.78°E, 27.81°N, 423 m	4729	168	T
Trisuli	85.04°E, 28.93°N, 5361 m	84.78°E, 27.81°N, 423 m	6610	230	B
		84.56°E, 27.85°N, 372 m	11,888	261	M
		84.46°E, 27.82°N, 303 m	16,810	274	S
		84.42°E, 27.74°N, 189 m	19,812	293	K
		Arun-Tamba Drainage System			
Arun	87.03°E, 28.59°N, 4291 m	87.16°E, 26.91°N, 160 m	33,507	341	R
		87.16°E, 26.91°N, 160 m	51,676	342	S
Tamur	88.12°E, 27.80°N, 5637 m	87.16°E, 26.91°N, 160 m	6058	199	A
Dudh	86.71°E, 28.08°N, 6375 m	86.43°E, 27.15°N, 338 m	4068	147	S
Tamba	86.30°E, 28.32°N, 5916 m	85.98°E, 27.35°N, 470 m	4134	143	S
Sun	85.64°E, 28.09°N, 4272 m	86.16°E, 26.91°N, 160 m	18,161	300	A
Poe Chu	86.05°E, 28.34°N, 4193 m	85.71°E, 27.63°N, 619 m	3401	109	S

(MBT). Although the initial motion along the STDZ is not well constrained, activity all along the strike of this structure is reported around 17 Ma [e.g., *Hodges et al.*, 1998; *Hodges*, 2000; *Searle et al.*, 1997, 1999]. Deformation related to the STDZ terminated about 10 ma ago, as crosscutting normal faults in southern Tibet show initial motion about 8–9 Ma ago [e.g., *Burchfiel et al.*, 1992].

[9] For the MCT it is generally believed that it was active in the Miocene and that motion terminated (and the extrusion of the Himalaya Crystalline Complex (HCC) stopped) when the main deformation propagated southward into the Indian foreland. During its activity a displacement of 140 km up to 500 km is reported [*Gansser*, 1964; *Schelling and Arita*, 1991; *DeCelles et al.*, 2002; *Robinson et al.*, 2006]. There is also strong evidence for a major reactivation during late Miocene to Pliocene time [*Harrison et al.*, 1997, 1998; *Robinson et al.*, 2003; *Catlos et al.*, 2001]. The Main Boundary Thrust (MBT) had its principal time of activity between about 11 and 5 Ma [*Burbank et al.*, 1996].

[10] Owing to the ongoing southward propagation of the deformation, shortening transferred to the Subhimalaya Unit into recently active structures like the Main Dun Thrust (MDT) or Main Frontal Thrust (MFT) [*Avouac*, 2003]. All of these structures probably sole into a common shallow north dipping decollement: the Main Himalayan Thrust [e.g., *Zhao et al.*, 1993]. The ages for the young southern structures come in part indirectly from the age of exhumation of the Lesser Himalaya (LH) and are therefore not very well constrained [*Meigs et al.*, 1995; *DeCelles et al.*, 1998; *Robinson et al.*, 2001]. However, on the basis of sedimentological and Nd isotope data the rapid exhumation of the Lesser Himalaya started about 12 Ma ago [*Huyghe et al.*, 2001]. The very general picture outlined above is a bit more differentiated when looking at the activity of individual structures in individual drainage basins.

2.1. Morphological and Geological Setting of the Individual Drainages

[11] The two drainage basins investigated here–the Kali-Gandaki and the Arun have very similar morphological characteristics (Figures 1b, 1c, and 1d). They both consist of 5 or 6 major rivers. The Kali-Gandaki Basin includes (from west to east) the Kali-Gandaki itself, the Seti, the Marsyandi, the Buri-Gandaki and the Trisuli Rivers. The Arun Basin includes (from west to east) the Sun Kosi, the Poe Chu, the Tamba Kosi, the Dudh Kosi, the Arun itself and the Tamur Rivers. Most individual rivers have a main channel length that is longer than 150 km, draining areas of at least 2000 km^2. In total, the Kali-Gandaki and Arun Basin areas are both about 40000 km^2 to 50000 km^2 (Table 1). As all tributaries to both drainage basins drain more less form north to south, these rivers cross all the structures mentioned above [e.g., *Lavé and Avouac*, 2001].

[12] These rivers also flow across the major morphological changes so obvious to the trekking tourist. The obvious physiographic transition (PT1) from High Himalayan topography to the flat Tibetan Plateau is also accompanied by changes in the channel characteristics (Figure 3). Coming from the Tibetan Plateau, most rivers flow across a significant knickpoint when entering the Himalayan realm at a channel elevation of about 3000 m to 4000 m. In this position many rivers also change from an alluvial upper reach to a bed rock channel [e.g., *Pratt-Sitaula et al.*, 2004]. The rivers then flow through the High Himalayas in steeply incised bedrock channels across the MCT and exit the High Himalayas at what is known as the PT2, the physiographic transition some tens of kilometers south of the MCT, into the lowlands [*Hodges et al.*, 2001]. Here, they change again from a bed rock to an alluvial channel. Many of the deposits in this alluvial part are 50–35 ka old corresponding to a time where the Monsoon was a maximum [*Pratt-Sitaula et al.*, 2004]. A second small reach of bed rock channels is

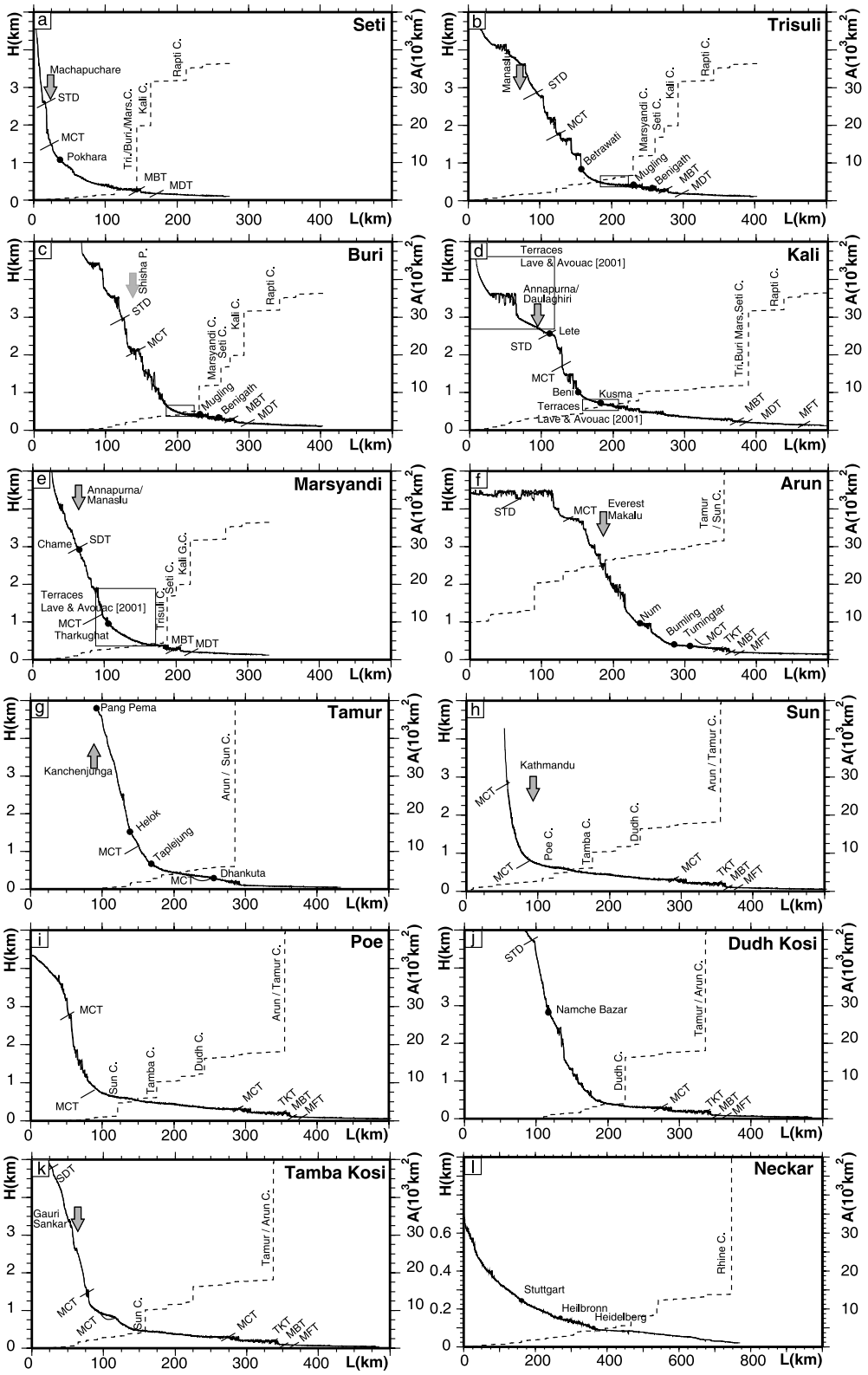

Figure 3. Channel profiles of major rivers in the Kali-Gandaki and Arun basins as shown on Figure 1b. The thin black line and thick black stand for the original channel profiles and for channel profiles filtered with a 10-km median filter, respectively. Dashed lines indicate the area distance relationship. Major confluence points are annotated. The position of major thrust and terraces are indicated. For a better orientation, important villages and high Himalayan peaks along the rivers are shown.

found where the rivers cross the Mahabarat range: the topographic front of the Himalayan orogen produced by uplift along the Main Boundary Thrust (MBT) and Main Dun Thrust. These thrusts are also likely to be responsible for damming [*Sakai et al.*, 2006] and bypassing [*Delcaillau et al.*, 2006] most of the south flowing Himalayan rivers to common confluence points as can also be shown for the Arun and Kali drainage basins.

[13] A detailed analysis of the incision rates and their changes along the channels of the rivers was performed by *Lavé and Avouac* [2001] using terrace elevations above the current streams. In particular, they showed that within the about 50 km wide zone of the High Himalayas, the incision is 4–8 mm per year while it is only 1–2 mm per year in the Lesser Himalaya south of the PT2. A comprehensive compilation of incision rates along major river channels, whole basins and the entire Himalayan range is given by *Montgomery and Stolar* [2006]. Interestingly, there is an abrupt discontinuity of the Ar/Ar cooling ages that corresponds with PT2 from hilly low landscape to the High Himalaya. This transition was first observed by *Copeland et al.* [1991] in the Buri drainage and has since been documented in most of the other rivers in the Kali-Gandaki system [*Wobus et al.*, 2006a]. This observation has given rise to a series of new interpretations on re-activation of the MCT system by an out-of-sequence thrust, on updoming of this region without breakthrough of faults to the surface and others (see discussion by *Wobus et al.* [2006a]). An alternative explanation of discontinuous Ar/Ar cooling ages is given by *Beyssac et al.* [2004] and *Bollinger et al.* [2006] who show that, with increasing distance to the MCT, Lesser Himalayan rocks did not reach temperatures higher than the closure temperature when they were accreted to the Himalayan wedge. The different models predict slightly different geometries of the uplift within the zone known to be uplifting, but data and models are as yet too sparse to allow a more detailed constraint on these different interpretations. In our modeling we attempt to constrain this somewhat further.

2.2. River Anticlines

[14] The formation of anticlines controlled by river incision and isostatic response represents the most apparent feedback between climate, erosion and large-scale deformation. River anticlines have been observed most prominently along major south draining Himalayan rivers [e.g., *Wager*, 1937], for example along the Indus [*DiPietro et al.*, 1999], Arun [e.g., *Meier and Hiltner*, 1993], the Yarlung Tsangpo [e.g., *Zeitler et al.*, 2001] and from several others (Sutlej, Kali-Gandaki, Karnali, Tista) [e.g., *Oberlander*, 1985]. These rivers follow the crest of the anticlines that are characterized by an amplitude of about 10 km and a wavelength between 30 and 80 km [*Montgomery and Stolar*, 2006]. Such a coupling between erosion and deformation can lead to the rise of mountain peaks [*England and Molnar*, 1990] and the formation of topography due to strong and local gradients in the uplift rate caused by tectonic response [*Zeitler et al.*, 2001; *Simpson*, 2006].

2.3. Main Channel Characteristics

[15] Channel profiles for the main south draining Himalayan rivers investigated here are shown in Figure 3. They show small channel gradients in the headwater whenever they originate within the Tibetan Plateau (Arun, Kali). This section is followed by a 50- to 80-km steep channel segment with a more less constant channel gradient (e.g., Marsyandi, Arun, Tamba Kosi) and an abrupt transition to very small channel gradients (Dudh Kosi, Tamba Kosi, Tamur) in the lower reaches near the common confluence. While the steep channel segments are generally characterized by bedrock channels within deep gorges, terraces are formed in both parts of the channels with small channel gradients [*Lavé and Avouac*, 2001]. Knickpoints that are not caused by major confluences coincide with the occurrence of recently active trust faults (MFT, MDT, MBT) but there seems to be no evidence for still existing knickpoints at the position of the MCT or STDZ where the last major motion is more than 10 ma ago. Some of the knickpoints have no geological relevance as they are caused by voids in the digital elevation model. However, even outside the knickpoints, the channel profiles of all Himalayan rivers shown in Figure 3 are unusual in as much as they contain major linear sections. In order to emphasize how different these profiles are from 'normal' equilibrium channels, the channel profiles of the Arun and Kali drainage system (Figures 3a–3k) are compared with the channel profile of a typical tributary of the Rhine River (Central Europe) of similar size: the Neckar (Figure 3l). The Neckar is characterized by steep channels near the spring, a concave channel profile and a smooth decrease of the channel gradient with increasing drainage area. Knickpoints in such channels occur where large tributaries discharge into the main channel and are a consequence of a sudden increase of the cumulative discharge.

[16] In order to unravel the significance of the atypical features of the channel profiles described above we show results of a detailed analysis of the digital elevation model of this region, compare numerically modeled- with measured channel profiles and present some 2-dimensional numerical models for different time slices using a simple erosion code.

3. Data and Numerical Model

[17] Our numerical model is based on version 2 of the SRTM3 data set, which was enhanced due post processing at NGA (National Geospatial-Intelligence Agency). The resolution of the digital elevation model is 3 arc seconds or about 90 m. Remaining voids in the data set were filled by the so-called minimum surfaces which can be computed as the solution of the Poisson equation with the surface heights at the border of the void as boundary values. In other words, the mean curvature of the surface at every point is zero ($d^2H/dx^2 + d^2H/dy^2 = 0$). This approach can be visualized replacing voids by soap films. This method shows advantages to standard interpolation methods as only a small number of additional closed basins (basins without an outlet) is introduced into the digital elevation model. In a

second step closed basins are filled until every point of the data set is characterized by a unique flow direction that allows the creation of a flow grid. Upstream drainage areas, river networks and drainage divides are calculated by a recursive approach, starting at the outlets (lowest points) at the geographic limits of the area and following the flow grid upstream to the ridges (highest points) of the DEM. The channel profiles shown on Figure 3 are calculated by defining the coordinates of the river spring and successively following the flow grid to the outlet. The thin black line shows the surface elevation of the river channel relative to the length of the channel measured from the spring by using the raw data after removing the voids but before filling the closed basins. It may be seen that the raw data fluctuate in certain areas, for example when gorges are too narrow to be resolved within the 3 arc seconds resolution of the digital elevation model or the exact surface elevation is missing caused by large voids. In order to reduce this noise, we applied a median filter with of 10 km wavelength to the river profiles (thick black line). This wavelength turned out to be a good compromise between reducing noise and preserving as much information as possible (Figure 3). The filtered river profiles are almost exclusively monotonous curves (going only downward) and are therefore the most practicable channel profiles that can be used for further modeling. These monotonous, equally spaced, median channel profiles will be our data set that we compare with numerical model curves. As we assume that the discharge of a river is proportional to the upstream drainage area (dashed lines), confluence points with large tributaries are characterized by steps in the line for the upstream drainage area and often by knickpoints in the channel profiles.

3.1. Model Description

[18] In order to compare measured with numerical modeled channel profiles, we have selected the most common detachment limited model to describe bedrock channel erosion [e.g., *Howard*, 1980; *Hergarten*, 2002] of the form

$$\left(\frac{\partial H}{\partial t}\right) = U - f\left(-A^{\theta}\frac{\partial H}{\partial L}\right). \quad (1)$$

Equation (1) describes the fluvial incision rate ($\partial H/\partial t$), as a power law function of the drainage area (A) and the channel gradient ($\partial H/\partial L$), where H is surface elevation, t is time, U stands for the uplift rate, and L represents the length of the channel segment. This model for detachment limited fluvial erosion bases on an empirical study of longitudinal river profiles, where *Hack* [1957] observed that the channel gradient is inversely proportional to the upstream drainage area of the river to the power of an exponent θ, i.e., the concavity index [*Flint*, 1974]. The concavity index controls the shape of steady state channel profiles and becomes therefore a crucial factor in modeling equilibrium channel profiles. Ôhe range of θ was determined between 0.25 and 0.6 [*Hack*, 1957].

[19] The erosion law from equation (1) is not only justified by empirical studies of river profiles, but can also be derived from theoretical principles. Assuming that the erosion rate is a function of basal shear stress [*Howard*, 1994], erosion rate can also be described as a function of the river discharge q instead of basin area, i.e., as a function of $q^{\theta}*\partial H/\partial L$. Depending on the approach, values between $\theta = 3/7$ and $\theta = 1/2$ are found (see *Tucker and Whipple* [2002] for a review). If precipitation is constant and mean discharge is used, this approach immediately leads to equation (1) with the same value of θ. If, however, the approach is based on other precipitation data, for example on decadal peak discharge [*Lavé and Avouac*, 2001], the exponent θ slightly changes since peak discharge was found to be proportional to $A^{0.89}$ instead of A. However, this change falls into the observed variation of θ, so that equation (1) with $\theta = 1/2$ is the simplest and most practical approach to model detachment limited fluvial erosion. The channel width is not treated explicitly, as it is assumed that the width of the channel is proportional to a power law function of the discharge in the form: q^b where b ranges between 0.3–0.5 [e.g., *Lavé and Avouac*, 2001] and is therefore subsumed in θ. However, *Finnegan et al.* [2005] have shown that the channel width is not only controlled by the discharge but also by the channel gradient, which leads to an underestimate of the stream power in rivers that steepen downstream.

[20] For a comparison between observed river profiles and numerically modeled ones we have followed a series of model steps that are increasingly refined with respect to the model assumptions made when interpreting equation (1). First, we have assumed that equilibrium prevails. In other words, we have modeled equilibrium channel profiles against which the real channel profiles can be evaluated. Differences can then be interpreted in terms of tectonic disturbances or lithologic variations. In equilibrium, the erosion rate at every point along the channel is constant ($\partial H/\partial t$ = const) as long as the uplift rate of the whole drainage system is a constant. Then equation (1) simplifies to the original formulation of *Hack* [1957].

$$\left(\frac{\partial H}{\partial L}\right) \propto -A^{-\theta}. \quad (2)$$

Equation (2) can be analytically solved by using empirical relationships between drainage area and (along-stream) distance from the river source [*Hack*, 1957]. However, in order to regard the effect of the river confluences, we use the real area-distance relations of the considered rivers shown in Figure 3 (dashed lines). We therefore solve the first-order differential equation (equation (2)) numerically using a backward (i.e., in upstream direction) finite difference scheme.

[21] Further, we define stream power s as the product

$$s = \left(-\frac{\partial H}{\partial L}\right)A^{\theta} = \text{const} \quad (3)$$

by reformulating equation (2). Variations in s can be interpreted in terms of tectonic or lithological anomalies.

It should be noted that the established definition of stream power is rather

$$s = \left(\left(-\frac{\partial H}{\partial L} \right) A^{\theta} \right)^{\alpha}, \quad (4)$$

but that the exponent α is not well constrained [*Whipple and Tucker*, 1999]. However, as we are rather interested in relative changes in the stream power, than in absolute values, the exponent α need not be considered. Equilibrium channel profiles numerically modeled with equations (2)–(4) can be compared with channel profiles of natural rivers and deviations between modeled and measured channel profiles can be interpreted in terms of the latest tectonic evolution of the region.

[22] In a second modeling step, time-dependent river profiles are computed. While the exact shape of the function f from equation (1) is irrelevant for equilibrium channel profiles, the temporal evolution depends on it. We therefore follow a simple power law approach where

$$f(s) = E * s^{n} = E \left(\left(-\frac{\partial H}{\partial L} \right) A^{\theta} \right)^{n}, \quad (5)$$

and E is a constant. The exponent n has a strong effect on the propagation of disturbances, but cannot be easily constrained from observations, so that values of n used in the literature vary more strongly than those of θ. *Hergarten and Neugebauer* [2001] used $n = 2$, while several other authors applied values close to $n = 1$, (see *Tucker and Whipple* [2002] for a review). Most models follow the assumption that s is linear proportional to the stream power so that $\alpha = n$ and we follow this here.

3.2. Determination of the Concavity Index

[23] Both the analytical and numerical approach to model equilibrium channel profiles are plagued by the uncertainties about the size of the exponent θ that ranges between 0.25 and 0.6 [*Hack*, 1957] but is more likely about 0.5 [*Tucker and Whipple*, 2002]. The θ may be derived from a double logarithmic plot of channel gradient against drainage area. *Wobus et al.* [2006b] have shown that in such a plot all points of a river segment in equilibrium with constant uplift define a straight line and that several river segments of different uplift can be described by several parallel straight lines where the channel gradient of the straight lines corresponds to $-\theta$ (Figure 4a). Beyond that, this relationship should be valid for all channels in the whole regions that are characterized by fluvial erosion, rather than by hillslope processes. To explore this relationship we use equation (5) and apply different uplift functions that show spatial variations but are constant over time (Figures 4a and 4b). The modeling is done until a steady state is reached. For a very simple situation in which a synthetic landscape is divided into a region of low and a region of high uplift, all points of the main river channel in the high uplifting region define a straight line and those in the low uplifting region another (Figure 4a, crosses). The slope of the two parallel straight lines describes the concavity index $\theta = 0.5$. If the uplift rate along the main channels varies spatially, this simple method to determine θ is not practicable. In a region that is characterized by highly variable uplift rates (sine shape uplift function), points along the main channel form an erratic track on the log-log plot (Figure 4b, crosses). In such a case it is not possible to determine θ directly from a single channel as it is hard to decide which data points share to same straight line. Then, a log-log density plot for the entire basin, where every data point of the basin is considered may be used to determine θ: The data points form a triangular shaped cloud with a well defined linear hull. In a steady state landscape the highest channel gradient at each drainage area class belongs to the region with the highest uplift rate. Therefore all these points on the linear hull share a common straight line where the slope represents $-\theta$. Ágain, it can be shown that θ exactly equals 0.5 (Figure 4b). For natural examples this method may be biased by the noise of the digital elevation model and by the fact that steady state is not fully reached. At least it should be possible to derive the possible range of θ which is done for the Tamur and Trisuli drainage systems (Figures 4c and 4d).

[24] The lower and the left hand limits of the data cloud are defined by the resolution of the digital elevation model as the minimum area of one cell is about 10^{-2} km^2 and the possible minimum slope of an integer-based 3 arc second DEM is 10^{-2}. Note, that the channel gradients for the main channels (crosses) can reach to lower values (10^{-3}) as for a noise reduction purpose the channel gradients were determined by a moving window approach with a step size of about 1 km. The enveloping tangent of the data cloud is inferred as data points in regions of maximum uplift in bedrock channels and represents one of several parallel straight lines characterized by a slope of $-\theta$ as defined in equation (2). It can be shown on Figure 4 that the linear hull is characterized by the same range of possible slopes between -0.50 and -0.33 in the two calculated sub basins of the Himalayan Rivers and are consistent with earlier results of *Hack* [1957] and *Lavé and Avouac* [2001]. The fits were done with the free eye, as any least square fits would require the elimination of problems with the digital elevation model (dots with very high channel gradients).

3.3. Equilibrium Channel Profiles

[25] The comparison of modeled and measured channel profiles (Figure 5) is instrumental to detect river segments of higher uplift relative to the other segments. The approach can also be used to define the state of equilibrium of a river channel. For this purpose we compare actual channel profiles of several north–south draining rivers of the Arun and the Kali drainage basins with their modeled counterparts.

[26] In order to illustrate that there is a good correspondence between modeled and measured channel profiles (usually not given in the Himalaya), Figure 5a shows this comparison for the Neckar River (Figure 5a) of central Germany. The channel profile numerically modeled for $1/\theta_{(\mathrm{mean})} = 2.5$ (dashed dotted line) (as determined in Figure 4) fits very well with the measured channel profile (solid line). We also determined the concavity index with

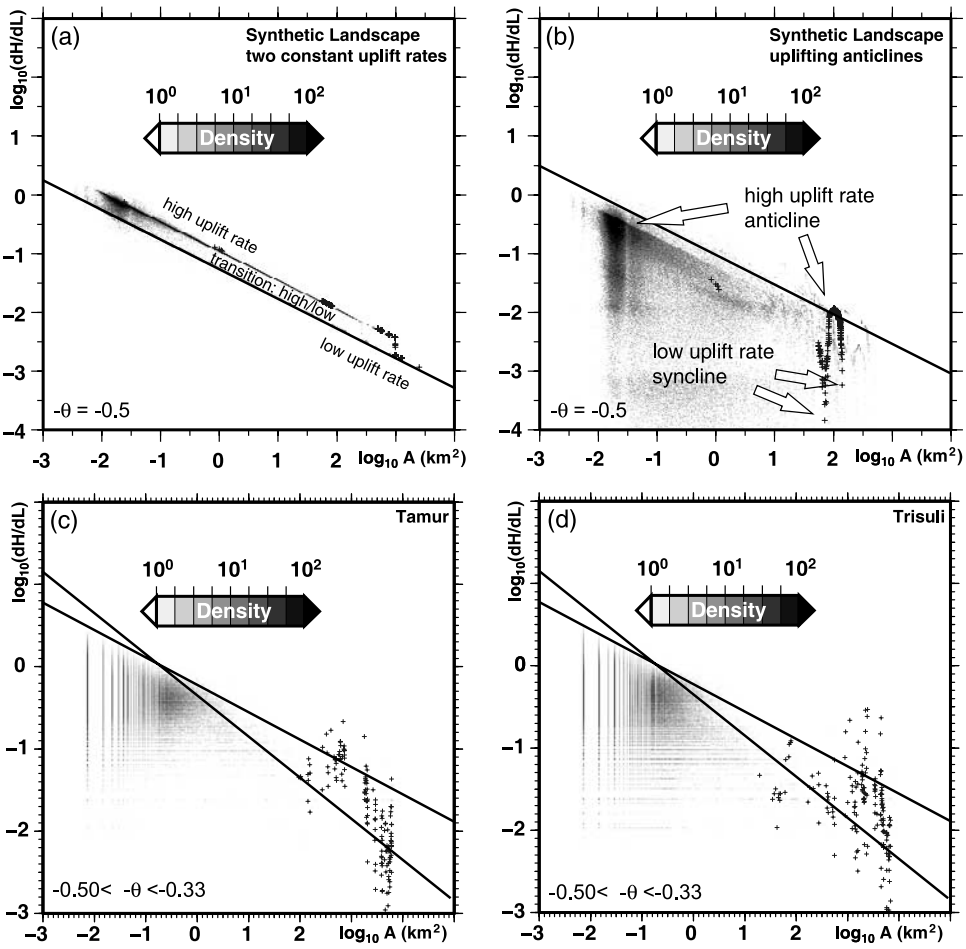

Figure 4. Channel gradient–area relationships for two synthetic landscapes and for two selected basins of the investigated area. (a) Steady state landscape characterized by two regions, one of high and one of low uplift rate. (b) Steady state landscape characterized by a sine-type uplift function forming synclines and anticlines. (c, d) Two natural examples from the Tamur and the Trisuli drainage system. The density indicates the frequency of data points in a grid of 100 × 100 classes for $\log_{10}(dH/dL)$ and $\log_{10}(A)$ for all points in the selected basin. The crosses show the distribution of data points along the main channel. To avoid noise caused by voids in the data set, a moving window algorithm with a step size of 1 km is used. The straight lines indicated the possible range of the concavity index θ.

another approach: by minimizing the difference in channel slope between numerically modeled and measured channel profiles (dashed line). The exponent derived from this least squares approach is $1/\theta = 1.953$ and lies only slightly below the range of exponents determined in Figure 4. The somewhat lower value for $1/\theta$ determined by this approach is caused by the pronounced knickpoint in the measured channel profile near the spring. Further, we show that that the Neckar River is in equilibrium and the whole main channel is uplifted by the same rate (except a small part in the headwaters). This fairly simple model can be successfully applied to actual rivers and deviations are caused by changing uplift rates along the channel.

[27] The original channel profiles of the Himalayan Rivers where cut so that the maximum and minimum elevation is 3500 m and 200 m, respectively (Figures 5b–5h). In general it can be seen that the correlation between the actual channel profiles with numerically derived channel profiles is poor for most of the rivers using an exponent of $1/\theta_{(mean)} = 2.5$. Even when fitting the exponent $1/\theta$ by minimizing the difference in channel slope between modeled and measured channel profiles the coincidence between model and nature is fairly bad. Despite of that, the derived exponents that should be valid globally vary significantly for the different Himalayan main channels between $1/\theta = 0.427$ (Seti) and $1/\theta = 1.617$ (Arun). If the exponent θ determined by the best fit approach differs dramatically from $1/\theta = 2.5$, the longitudinal channel profile may be interpreted in terms of lithological changes or even more likely in terms of variable spatial uplift rates.

[28] Several authors have shown that there is a corridor between PT1 and PT2 that is rapidly uplifted [e.g., *Lavé and*

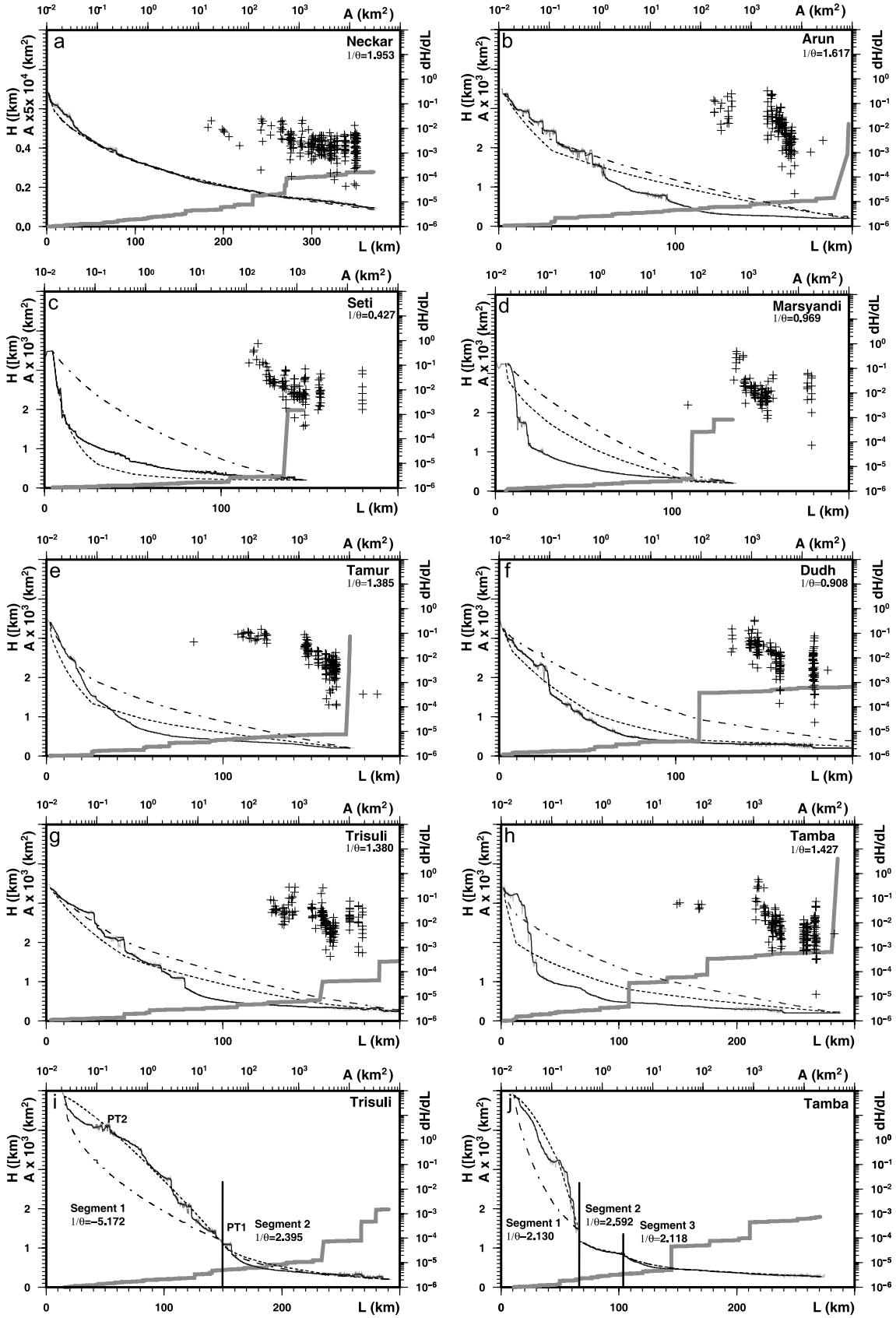
a
Neckar
1/θ=1.953
b
Arun
1/θ=1.617
c
Seti
1/θ=0.427
d
Marsyandi
1/θ=0.969
e
Tamur
1/θ=1.385
f
Dudh
1/θ=0.908
g
Trisuli
1/θ=1.380
h
Tamba
1/θ=1.427
i
Trisuli
PT2
PT1
Segment 1
1/θ=−5.172
Segment 2
1/θ=2.395
j
Tamba
Segment 1
1/θ=2.130
Segment 2
1/θ=2.592
Segment 3
1/θ=2.118
A (km²)
H ([km)
A x5x 10⁴ (km²)
A x 10³ (km²)
dH/dL
L (km)

Figure 5

Avouac, 2001]. If the uplift rate in this corridor is largely constant, as could be expected in case the uplift is tectonically driven, it should be possible to split the channel profiles into two or more segments and model each of these channel segments separately (Figures 5i and 5j). To test this we have chosen the Trisuli (Kali drainage basin) and the Tamba (Arun drainage basin) and have split the two rivers in 2 and 3 channel segments respectively. The channel segments below PT2, annotated as "segment 2" for the Trisuli River and "segment 3" for the Tamba River coincide nicely with the modeled profiles and the exponents determined by our approach to minimize the error in channel gradient are within a realistic range. For the Tamba River the channel below PT2 has to be split into two further segments as indicated by a striking knickpoint. "Segment 2" of the Tamba River shows also a very good correlation with the model suggesting a different but constant uplift rate relative to "segment 3." However, there is no way to successfully model the channel segments upstream of PT2 with our simple approach for both the Trisuli and the Tamba. In segment 1 the slope along the channel increases with increasing drainage area leading to negative best fit exponents to describe these convex channel segments. Other Himalayan rivers (e.g., Arun, Tamur) are characterized by a more or less linear relationship between channel length and channel elevation within this channel segment (Figure 5). Such an anomalous linkage between channel length, drainage area and channel gradient cannot be explained by simply uplifting one area relative to another and must indicate strong variation in uplift rate along the channel.

3.4. Stream Power

[29] To explore spatial variations of the surface uplift, calculations on the stream power (s) (Figure 6a) and the channel slopes ($\partial H/\partial L$) (Figure 6b) of the Arun and the Kali drainage basin were performed. In a state of equilibrium, the stream power in a channel is constant as long as the uplift rate is constant and there are no local variations in the precipitation so that q is proportional to upstream area, which is assumed here. In other words, variations in the stream power can be used to map regions of higher and lower uplift, which should give some evidence whether the uplift is controlled by plate-scale tectonics or is caused by erosion and river incision. In our calculations we used $1/\theta = 2.0$ for reasons discussed above. We also did the calculations for $1/\theta_{(\mathrm{mean})} = 2.5$ but found no significant differences. On Figure 6a it can be seen that the stream power of the drainage network is fairly constant, except for a 50 km to 80 km wide southeast northwest striking corridor where the stream power is increased by more than 1 order of magnitude. The corridor of maximum stream power corresponds roughly to the area suggested to be rapidly uplifting and is characterized by high erosion rates. Here we use the rates of river incision of the main channels determined by *Lavé and Avouac* [2001] to convert values for stream power to incision rates for the Kali-Gandaki and the Arun drainage network. For this, we have pinned an erosion rate of 10 mm a^{-1} for channel segments showing the highest stream power in the main channels and have determined the corresponding erosion rates for the whole drainage basin from this using $n = 1$ and $n = 2$ (equation (5)). Although such a conversion allows just a ballpark estimation of the spatial variations of the erosion rates for the entire network, the determined erosion rates of the main channels coincide nicely with those determined by *Lavé and Avouac* [2001]: they have a first maximum when crossing the High Himalayan Range and a second at the position of the recently active trusts in the Subhimalaya Unit. Values for high stream power and therefore elevated river incision north of the High Himalayan Range, in particular the northern tributaries of the Arun River are biased by the assumption of uniform precipitation, as this region is known to be dry.

[30] Tributaries that drain into the Arun, Tamba or Trisuli and run entirely within this strip of elevated stream power show increasing stream power in direction to the confluence points (Figures 6a and 7: t1–t4). These channels are also characterized by channel gradients that increase anomalously with increasing channel length (Figures 6b and 7: t1–t4). In detail, channel profiles for the tributaries t1–t4 are characterized by low gradient headwaters, a pronounced knickpoint located about 25 km to 30 km from the confluence point and a segment which shows increasing channel gradient with increasing channel length and area (Figures 7a–7d). The length of this segment is about 25 km to 30 km for all four tributaries. Tributaries of a similar length located about 100 km further south (Figures 6 and 7: t5–t6) show a completely different behavior. t5 originates within the zone of high stream power but drains north–south and confluences about 50 km south of this corridor (Figure 7e). The channel profile turns form a slightly convex to a concave curve at a channel length of about 20 km, somewhat south of the point where the river leaves the corridor of high stream power. As for the large north–south draining rivers, the channel profile cannot be modeled satisfyingly as a whole. Even for segment 1 the modeled profile diverges significantly from the measured. For segment 2 there is at least a very good fit between the modeled and measured channel segment (Figure 7e, inset). Tributary (t6) drains entirely south of the zone of high stream power (Figure 7f). The complete channel profile is characterized by a concave

Figure 5. Comparison of channel profiles of several main channels of the investigated area with numerically modeled channel profiles. The thin gray line indicates the raw data channel profile; the solid line on the top represents the filtered channel profile using a median filter as described in Figure 3. The thick gray line shows the distance-area relationship; the crosses show the area-channel gradient relationship. The dash-dotted line represents the numerical solution for the exponent of $1/\theta_{(\mathrm{mean})} = 2.5$ as determined in Figure 4. The dashed line shows a numerically modeled channel profile where the error in channel gradients between the modeled and the measured channel profile reaches a minimum. The concavity index θ, which is alternatively determined by this approach, is indicated top right in each diagram just below the name of the main channel.

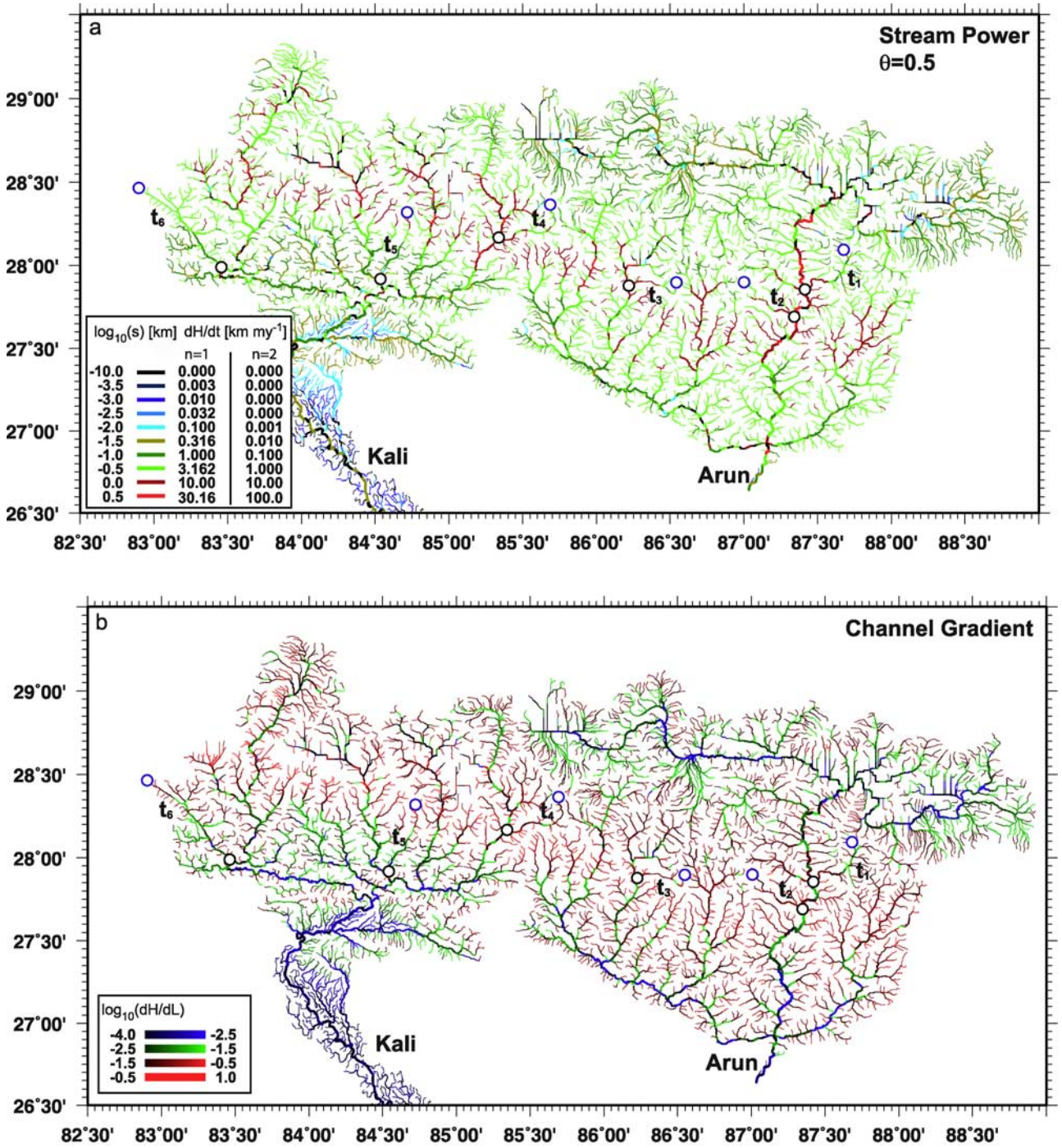

Figure 6. Maps showing (a) the stream power and (b) the channel gradients of the drainage network of the Kali-Gandaki and the Arun. Erosion rates determined by *Lavé and Avouac* [2001] were used to scale to stream power in terms of erosion rates for $n = 1$ and $n = 2$. To minimize the noise of the digital elevation model a moving window with a size of 4 km was applied to calculate the channel gradients. Blue and black circles mark the starting and endpoints for channel profiles of selected tributaries (t1–t6) shown in Figure 7.

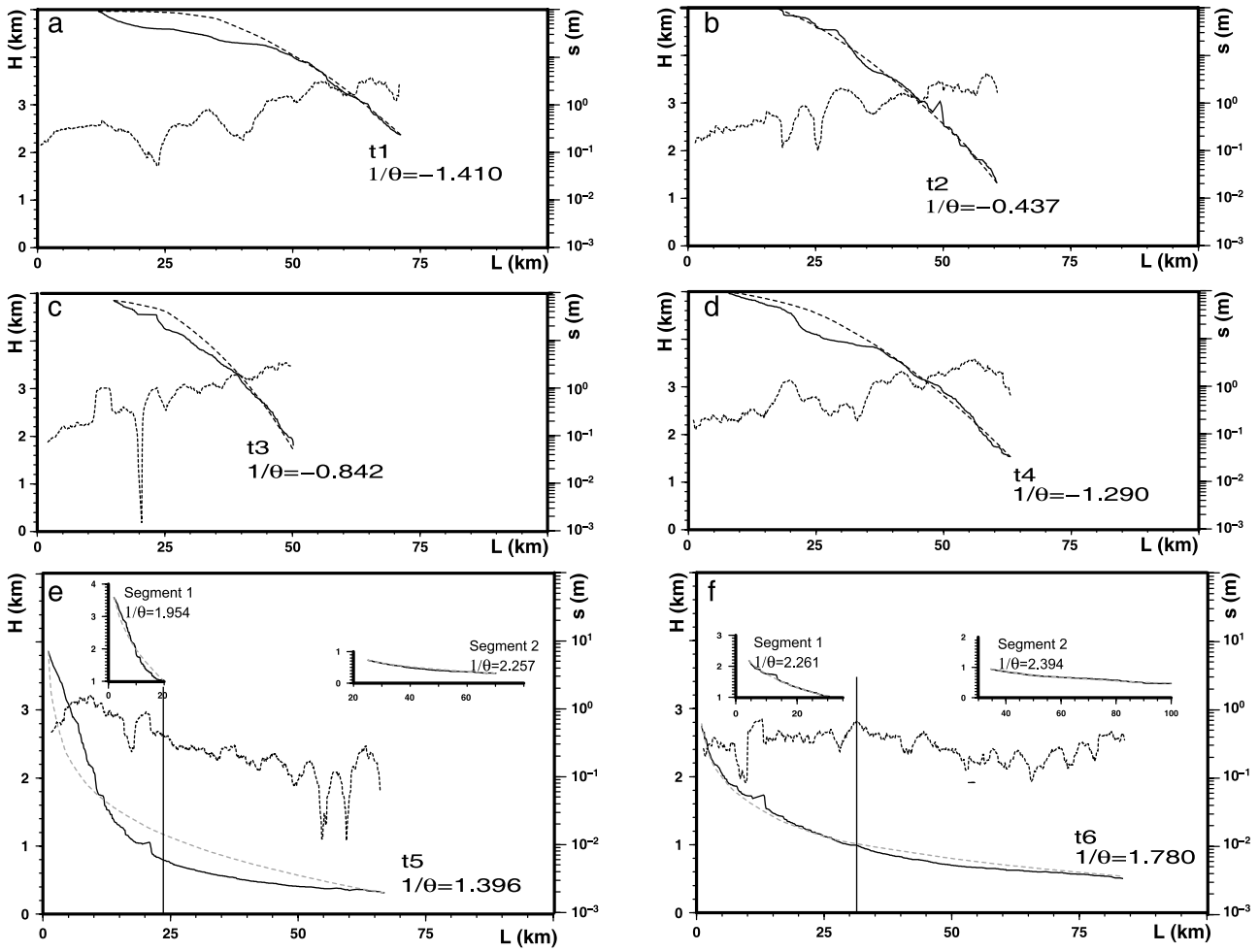

Figure 7. Measured and modeled best fit channel profiles of six tributaries of the Arun and Kali drainage systems as annotated in Figure 6 (t1–t6). Thin solid and thin dashed lines represent the measured and modeled (best fit) channel profiles, respectively. The best fit exponent is annotated at lower limit of the profiles. The dotted line stands for the stream power along the longitudinal channel profile using a moving window approach with a step size of 1 km. Insets in Figures 7e and 7f represent segments of the channel profile and their modeled counterpart.

shape and the modeled best fit profile diverges only slightly from the measured profile. By splitting the channel into two segments the coincidence between model and nature is excellent (Figure 7f, inset).

4. Discussion

[31] Figures 5, 6 and 7 express a clear picture on relative spatial variation of the uplift in the Kali and Arun drainage basins and allow a discussion of the nature of uplift in this region. Maps for stream power, channel gradients and channel profiles allow to define a corridor of elevated stream power, coinciding with a zone of young cooling ages [e.g., *Wobus et al.*, 2006a] and high incision rates [e.g., *Lavé and Avouac*, 2001]. However, such a strip of elevated stream power still allows both interpretations (tectonic versus erosional control) on the nature of uplift within this corridor.

4.1. Tectonic Versus Erosional Control of Elevated Uplift

[32] Rivers draining perpendicular to such a corridor of constant but elevated uplift should be characterized by concave channel profiles and knickpoints when entering and leaving this zone of higher uplift. Nevertheless, the channel gradient will decrease from the spring to the confluence point and the stream power along the river channel should be constant outside the corridor of high uplift and also constant (but higher) within this zone. In contrast, linear or convex river profiles in this zone of uplift (Figure 5) would require strong and local variations of the uplift rate perpendicular to this corridor. For example, if the zone of uplift is driven by tectonic channel-flow extrusion [e.g., *Grujic et al.*, 1996], the rate of uplift should be highest in the center of the uplifting zone. This model can provide a tectonic interpretation of linear or convex river channel profiles.

[33] Even more detail on the nature of uplift in this region is stored in tributaries that drain more or less orogen-parallel, entirely within the corridor of elevated stream power and perpendicular to the large rivers. An uplifting corridor driven by large-scale tectonics causes a region of elevated but relatively constant stream power in all these orogen parallel channels draining within this corridor. Even if uplift within this zone started recently and there is no equilibrium, channel profiles should still have a concave shape with knickpoints dividing the rivers in segments representing an equilibrium before and during the uplift. However, these channels are characterized by convex channel profiles, and are featured by increasing stream power and channel gradients from the springs the confluence points. These observations allow a simple interpretation: the uplift increases in direction to the main channels and the point of maximum uplift is focused in the main channels. It is very unlikely that tectonically driven uplift leads to convex channel profiles and increasing stream power in direction to the main channels. This would require that the uplift rate increases linearly in time so that the channel profiles consist of a series of moving knickpoints. Following the theory of knickpoint migration, kick points move with a constant vertical rate [*Wobus et al.*, 2006b] so that changes in the stream power pattern should be related to the surface elevation, which is not evident in the Arun or Kali-Gandaki drainage system.

[34] We therefore interpret the fact that east–west oriented tributaries to the main rivers have convex river profiles, as evidence for uplift driven by the incision of rivers as shown in Figure 2b. During the temporal evolution of the drainage system, it can be expected that the tendency of rivers to an equilibrium state cause an upstream directed shift of the physiographic transitions, as observed in escarpments all around the world, and it is likely that the zone of elevated stream power migrates in north direction. This will lead to the formation of river anticlines during the temporal evolution of the south draining Himalayan river system and can also explain the existence of river anticlines along river segments where currently no elevated stream power is observed and the channels have reached a state of equilibrium (e.g., Arun river segment in the Lesser Himalaya).

4.2. Temporal Constraints on the River Evolution

[35] The appearance of river anticlines around large north–south draining Himalayan rivers is not confined to the two drainage basins discussed here. The most important river anticlines have been reported around the Indus, Sutlej, Karnali, Arun and Yarlung Tsangpo [*Oberlander*, 1985]. *Montgomery and Stolar* [2006] have demonstrated that the elastic parameters of the Himalayan lithosphere would allow that these anticlines do indeed form as an isostatic response to incision. Numerical models that couple erosion, deposition and thin plate deformation show that the formation of large anticlines can be driven by high erosion rates [e.g., *Simpson*, 2006]. S. Hergarten (personal communication, 2008) show numerically that the feedback between river incision and viscous deformation causes local uplift around large rivers up to several 1000 m for a realistic range of viscosities ($\sim 10^{22}$ Pas). However, aside from suggestions of *Meier and Hiltner* [1993] who argued that these anticlines are the youngest feature of the deformation history, few authors have attempted to constrain the formation of these anticlines in time.

[36] Interestingly, rivers with pronounced anticlines have in common that a substantial part of their drainage area is located north of the High Himalayas, within the Tibetan Plateau. This nourishes the suspicion that the beginning of accelerated formation of these anticlines correlates with the time of breakthrough of head-ward cutting drainages into the Tibetan Hinterland, capturing previously west–east draining systems. This would abruptly increase their stream power and therefore the erosion rates in the steep channel segments. Today, the region north of the Himalayan chain is extremely dry, so that capture of the streams in this region does increase the basin area substantially, but not necessarily the stream power. However, several authors have shown that the lack of precipitation on the Tibetan Plateau is a relatively recent feature with a substantially wetter climate over much of the Quaternary [e.g., *Zhang et al.*, 2007; *Gasse et al.*, 1991].

[37] To illustrate the possibility that head-ward cutting of rivers caused the capture of west–east running rivers north of the Himalayan range, we have performed a series of time-dependent models for the central Himalaya with our 2-dimensional numerical erosion code (Figure 8). The model, discussed in detail by Stüwe et al. (submitted manuscript, 2008), uses equation (5) and an erodibility of $E = 50\ \mathrm{km^{-1}my^{-1}}$, $\theta = 0.5$ and $n = 2$, so that the erosion rates of the model coincide largely with the rates for river incision determined by *Lavé and Avouac* [2001]. Note, that this E is about 1 order of magnitude higher than that determined as an average for the whole Tibetan Plateau (Stüwe et al., submitted manuscript, 2008). The high erosion rates determined by *Lavé and Avouac* [2001] are accompanied by high uplift rates that are not considered in this rather simple model, so that the overall erodibility may therefore be overestimated.

[38] However, in models that describe a relaxing topography without uplift or deformation, the erosion rate scales linearly with time so that downscaling the erosion rate by 1 order of magnitude would result in a 10 times longer time span and an erodibility of $E = 5\ \mathrm{km^{-1}ma^{-1}}$, without changing the morphometric geometry. Furthermore we have interpolated a digital elevation model for the Himalayan range onto a triangulated mesh. In order to model the time-dependent evolution of rivers since before they break through to the Tibetan Plateau, the digital elevation model of this region is filtered and subbasins on the north side of the High Himalayas are cut off by introducing artificial barriers. As there is no information on Miocene topography, barriers are arbitrarily inserted, so that we can explore the process of head-ward cutting and capturing. Figure 8 shows a cartoon like model illustration of the drainage development in the orogen, although some rivers very much look like the real geometry. To keep the model simple we have not implemented any uplift and use this model only to illustrate the head-ward cutting of Himalayan rivers and to

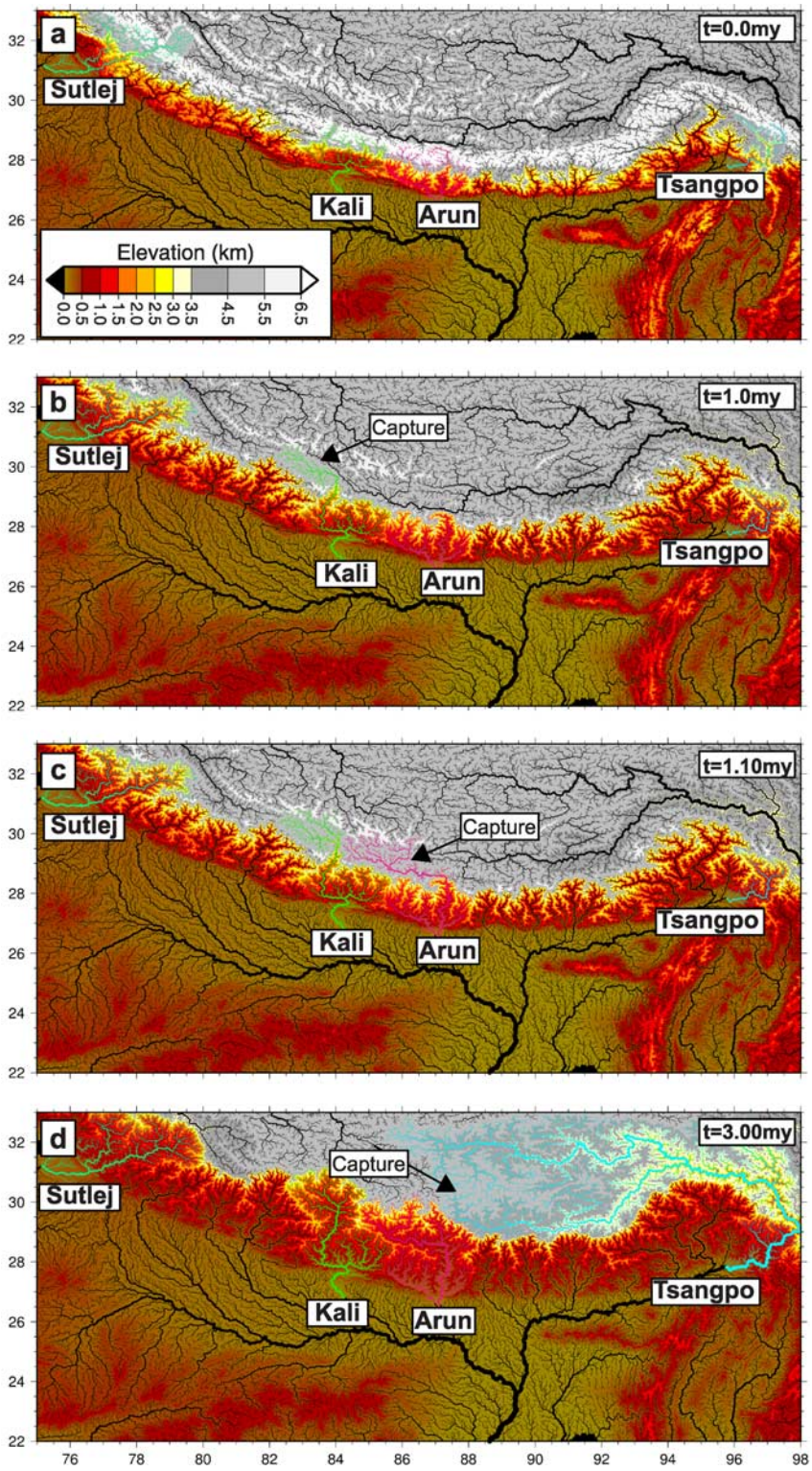

Figure 8. Four time steps of a time-dependent model evolution illustrating the capture of west–east running rivers north of the Himalayan chain by rivers draining into the Ganges plain. The model evolution is run over about 3 ma using equation (1) with $E = 50$ km^{-1}a^{-1}, $1/\theta = 2$ and $n = 2$. As the erosion rate in this model scales linear with time, the same model can be interpreted for E = 5 km^{-1}a^{-1} and for a timespan of 30 ma by lowering the erosion rates by 1 order of magnitude. In order to mimic the situation some millions of years ago (Figure 8a), a synthetic barrier was built into the region of the High Himalayas.

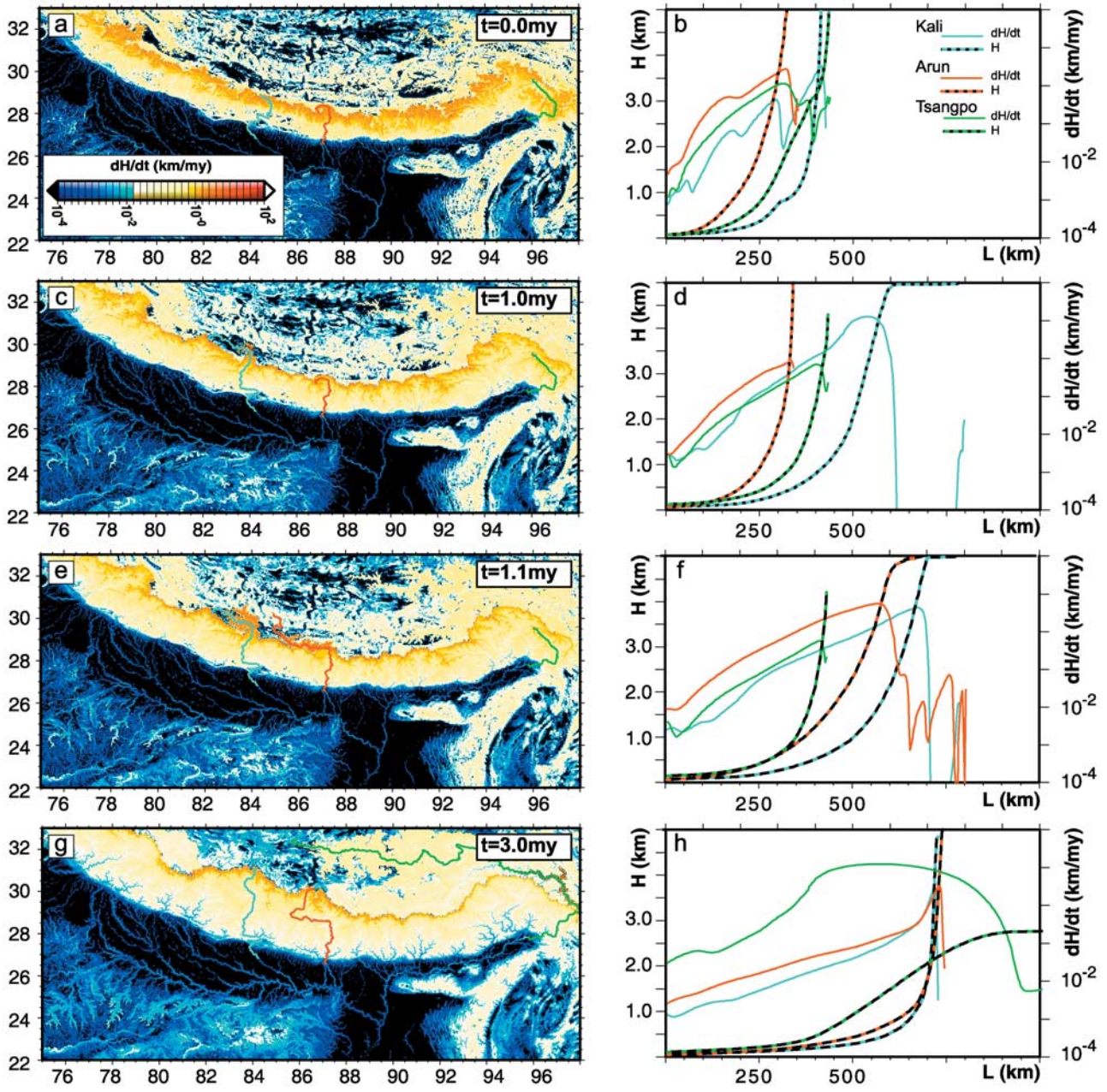

Figure 9. The correlation between capture of west–east draining rivers and erosion rates for the same model run presented in Figure 8. Upstream channel profiles (dashed lines) and upstream profiles for the erosion rate (solid lines) along the "Kali," "Arun," and "Yarlung Tsangpo" are presented for four different time slices.

explore how the erosional front will develop with time. Figure 8a illustrates the initial situation of the model run. The Kali-Gandaki system (in green) is actually similar in its geometry as it is today. The Arun, the Yarlung Tsangpo and the Sutlej system all do not traverse the range in Figure 8a, but only drain the Himalayas to the south. After 1.0 ma and 1.1 ma the Kali-Gandaki and the Arun capture west–east running rivers in the north of the Himalayas, respectively. After 3.0 ma the originally west–east draining Yarlung Tsangpo is captured. Capturing occurs because the east–west running river are characterized by very small channel gradients, low erosion rates and a high base level, while the north–south draining rivers have very high erosion rates and a low base level. This causes head-ward cutting of the south draining rivers into the Tibetan Plateau and a rapid shift of the drainage divide toward the north. We conclude that many of the trans-Himalayan rivers may not be antecedent, but are the consequence of rapid headward migration of rivers draining the Himalayas to the south.

[39] The timing of the capture events within this model setup is hard to interpret as it is highly influenced by the geometry of the artificial barriers. Over time the originally linear steep front of the range (Figure 8a) decays increasingly. This is caused by different rates of backward cutting and capturing of rivers in the Tibetan Plateau. As a consequence the front of the range becomes increasingly broken up. Note that the same model runs performed for $n = 1$ cause also backward cutting, capturing and the destruction of the linear front of the Himalayan range, but the rates of the backward cutting and the channel characteristics are significantly different. As this model result contradicts the field observation that the front remained reasonably linear, we propose that the uplift within a 50- to 80-km-wide southeast northwest striking zone caused this linear front. This also slows down the backward cutting of rivers. This process is also suggested by *Zeitler et al.* [2001] for the Yarlung Tsangpo forming a distinct river anticline after the river was captured by the Brahmaputra.

[40] Nevertheless, we can expect that during the process of headward cutting over time, the position of maximum stream power and highest erosion rates will migrate in north direction as well, which, as a consequence, should shift the activity of river anticlines in the same direction (Figure 9). Capturing events can be correlated with an abrupt rise of the erosion rate downstream the capturing channel, as can seen by comparing the maps and profiles for the erosion rate of the Kali before (Figures 9a and 9b) and after (Figures 9c and 9d) the capture event, of the Arun (Figures 9c and 9d) and (Figures 9e and 9f) and even more extreme for the Yarlung Tsangpo (Figures 9e–9h). The extreme rise of the erosion rate after the capture event causes rapid flattening of the channel profiles within a time span below 1 ma. Here again, it should be noted that, taking a zone of rapid uplift into consideration, the channel gradients and erosion rates would remain much higher for a longer time span, while rate of the north directed migration of the erosion front would be significantly reduced. Back to the formation of river anticlines, we propose that capturing of large orogen parallel rivers within the Tibetan Plateau can significantly accelerate the growth of river anticlines. Of course, the impact of this process depends highly on the precipitation within the Tibetan Plateau and the discharge of Tibetan rivers during the last million years which is still subject of speculations.

5. Conclusion

[41] We propose a model for the formation of Himalayan river anticlines, where they form in response to river incision. Their formation was accelerated when backward cutting of south draining Himalayan rivers into the Tibetan Plateau captured additional drainage basins. The model stems from the following more detailed conclusions.

[42] 1. From double logarithmic plots channel gradient against drainage area for several sub basins of the Kali-Gandaki and the Arun drainage system we could determine a range for the exponent θ between 0.5 and 0.33.

[43] 2. Using an exponent $\theta_{(mean)} = 0.4$ and model equilibrium channel profiles for several large south draining Himalayan rivers, the coincidence between measured and modeled channel profiles is poor. Splitting the channels into several segments allow successfully modeling the segments below PT2. Best fit exponents for the segments between PT1 and PT2 show often negative values caused by a convex channel profile within this segment.

[44] 3. Calculating the stream power and the channel gradients of the drainage network of the Kali and the Arun, an about 50- to 80-km-wide southeast northwest striking zone can be mapped with elevated stream power by more than 1 order of magnitude and significantly larger channel gradients. Tributaries draining parallel to that zone show increasing stream power and increasing channel gradient from the spring the confluence point.

[45] 4. Convex channel profiles of such tributaries are common. Together with convex channel segments of south draining rivers that cross this zone, we can localize regions of maximum uplift exactly within the channels of large Himalayan rivers and can also conclude that the uplift decreases with increasing distance to the main channels. As this cannot be by incident, we conclude that a significant amount of uplift within this corridor is driven by river incision.

[46] 5. Time-dependent model runs show that the Himalayan rivers are characterized by rapid headward cutting toward the Tibetan Plateau. During their evolution, rivers capture east–west running rivers from the north of the High Himalayas causing sudden increases in stream power of these rivers.

[47] 6. We propose that this rapid increase in stream power may be responsible for increased incision, isostatic rebound and ultimately for an accelerated formation of the river anticlines observed around several of the trans-Himalayan rivers.

[48] **Acknowledgments.** This project was supported by the FWF-P18341. This paper benefited greatly by the detailed and constructive reviews by J.P. Avouac and an anonymous reviewer.

References

Avouac, J. P. (2003), Mountain building, erosion, and the seismic cycle in the Nepal Himalaya, *Adv. Geophys.*, *46*, 1–80.

Avouac, J. P., and P. Tapponier (1993), Kinematic model of active deformation in central Asia, *Geophys. Res. Lett.*, *20*, 895–898, doi:10.1029/93GL00128.

Beaumont, C., R. A. Jamieson, M. H. Nguyen, and S. Medvedev (2004), Crustal channel flows: 1. Numerical models with applications to the tectonics of the Himalayan-Tibetan orogen, *J. Geophys. Res.*, *109*, B06406, doi:10.1029/2003JB002809.

Beyssac, O., L. Bollinger, J.-P. Avouac, and B. Goffe (2004), Thermal metamorphism in the lesser Himalaya of Nepal determined from Raman spectroscopy of carbonaceous material, *Earth Planet. Sci. Lett.*, *225*, 233–241, doi:10.1016/j.epsl.2004.05.023.

Bollinger, L., P. Henry, and J. P. Avouac (2006), Mountain building in the Nepal Himalaya: Thermal and kinematic model, *Earth Planet. Sci. Lett.*, *244*, 58–71, doi:10.1016/j.epsl.2006.01.045.

Burbank, D. W., R. A. Beck, and T. Mulder (1996), The Himalayan foreland basin, in *The Tectonics of Asia*, vol. 88, edited by A. Yin and M. Harrison, pp. 149–188, Cambridge Univ. Press, New York.

Burchfiel, B., C. Z. Chen, K. V. Hodges, Y. Liu, L. H. Roysen, C. Deng, and J. Xu (1992), The South Tibetan detachment system, Himalayan orogen:

Extension contemporaneous with and parallel to shortening in a collisional mountain belt, *Spec. Pap. Geol. Soc. Am.*, *269*, 41 pp.

Catlos, E. J., T. M. Harrison, M. J. Kohn, M. Grove, F. J. Ryerson, C. Manning, and B. N. Upreti (2001), Geochronologic and thermobarometric constraints on the evolution of the Main Central Thrust, central Nepal Himalaya, *J. Geophys. Res.*, *106*, 16,177–16,204, doi:10.1029/2000JB900375.

Chung, S.-L., C.-H. Lo, T.-Y. Lee, Y. Zhang, Y. Xie, X. Li, K.-L. Wang, and P.-L. Wang (1998), Diachronous uplift of the Tibetan plateau starting 40 Myr ago, *Nature*, *394*, 769–773, doi:10.1038/29511.

Copeland, P., T. M. Harrison, K. V. Hodges, P. Maruejol, P. LeFort, and A. Pecher (1991), An early Pliocene thermal disturbance of the Main Central Thrust, central Nepal: Implications for Himalayan tectonics, *J. Geophys. Res.*, *96*, 8475–8500, doi:10.1029/91JB00178.

DeCelles, P. G., G. E. Gehrels, J. Quade, T. P. Ojha, P. A. Kapp, and B. N. Upreti (1998), Neogene foreland basin deposits, erosional unroofing and the kinematic history of the Himalayan fold-thrust belt, western Nepal, *Geol. Soc. Am. Bull.*, *110*, 2–21, doi:10.1130/0016-7606(1998)110<0002:NFBDEU>2.3.CO;2.

DeCelles, P. G., D. M. Robinson, and G. Zandt (2002), Implications of shortening in the Himalayan fold-thrust belt for uplift of the Tibetan Plateau, *Tectonics*, *21*(6), 1062, doi:10.1029/2001TC001322.

Delcaillau, B., J. M. Carozza, and E. Laville (2006), Recent fold growth and drainage development: The Janauri and Chandigarh anticlines in the Siwalik foothills, northwest India, *Geomorphology*, *76*, 241–256, doi:10.1016/j.geomorph.2005.11.005.

DiPietro, J. A., K. R. Pogue, A. Hussain, and I. Ahmad (1999), Geologic map of the Indus syntaxis and surrounding area, Northwest Himalaya, Pakistan, *Spec. Pap. Geol. Soc. Am.*, *328*, 159–178.

England, P. C., and G. A. Houseman (1989), Extension during continental convergence, with application to the Tibetan plateau, *J. Geophys. Res.*, *94*, 17,561–17,579, doi:10.1029/JB094iB12p17561.

England, P. C., and P. Molnar (1990), Surface uplift, uplift of rocks, and exhumation of rocks, *Geology*, *18*, 1173–1177, doi:10.1130/0091-7613(1990)018<1173:SUUORA>2.3.CO;2.

Finnegan, N. J., G. Roe, D. R. Montgomery, and B. Hallet (2005), Controls on the channel width of rivers: Implications for modeling fluvial incision of bedrock, *Geology*, *33*, 229–232, doi:10.1130/G21171.1.

Flint, J. J. (1974), Stream gradient as a function of order, magnitude, and discharge, *Water Resour. Res.*, *10*, 969–973, doi:10.1029/WR010i005p00969.

Gansser, A. (1964), *Geology of the Himalayas*, 289 pp., Wiley Intersci., London.

Gasse, F., et al. (1991), A 13,000 year climate record from western Tibet, *Nature*, *353*, 742–745, doi:10.1038/353742a0.

Grujic, D., M. Casey, C. Davidson, L. S. Hollister, R. Kuendig, T. L. Pavlis, and S. M. Schmid (1996), Ductile extrusion of the Higher Himalayan Crystalline in Bhutan; Evidence from quartz microfabrics, *Tectonophysics*, *260*, 21–43, doi:10.1016/0040-1951(96)00074-1.

Grujic, D., I. Coutand, B. Bookhagen, S. Bonnet, A. Blythe, and C. Duncan (2006), Climatic forcing of erosion, landscape, and tectonics in the Bhutan Himalayas, *Geology*, *34*, 801–804, doi:10.1130/G22648.1.

Hack, J. T. (1957), Studies of longitudinal stream profiles in Virginia and Maryland, *U. S. Geol. Surv. Prof. Pap.*, *294B*, 45–97.

Harrison, T. M., F. J. Ryerson, P. LeFort, A. Yin, O. Lovera, and E. J. Catlos (1997), A late Miocene-Pliocene origin for the central Himalayan inverted metamorphism, *Earth Planet. Sci. Lett.*, *146*, E1–E7, doi:10.1016/S0012-821X(96)00215-4.

Harrison, T. M., M. Grove, O. M. Lovera, and E. J. Catlos (1998), A model for the origin of Himalayan anatexis and inverted metamorphism, *J. Geophys. Res.*, *103*, 27,017–27,032, doi:10.1029/98JB02468.

Hergarten, S. (2002), *Self organised criticality in Earth Systems*, 272 pp., Springer, Heidelberg.

Hergarten, S., and H. J. Neugebauer (2001), Self-organized critical drainage networks, *Phys. Rev. Lett.*, *86*, 2689–2692, doi:10.1103/PhysRevLett.86.2689.

Hodges, K. V. (2000), Tectonics of the Himalaya and southern Tibet from two perspectives, *Geol. Soc. Am. Bull.*, *112*, 324–350, doi:10.1130/0016-7606(2000)112<0324:TOTHAS>2.3.CO;2.

Hodges, K. V., S. A. Bowring, K. L. Davidek, D. Hawkins, and M. Krol (1998), Evidence for rapid displacement on Himalayan normal faults and the importance of tectonic denudation in the evolution of mountain ranges, *Geology*, *26*, 483–486, doi:10.1130/0091-7613(1998)026<0483:EFRDOH>2.3.CO;2.

Hodges, K. V., J. M. Hurtado, and K. X. Whipple (2001), Southward extrusion of Tibetan crust and its effect on Himalayan tectonics, *Tectonics*, *20*, 799–809, doi:10.1029/2001TC001281.

Howard, A. D. (1980), Thresholds in river regimes, in *Thresholds in Geomorphology*, edited by D. R. Coates and J. D. Vitek, pp. 227–258, Allen and Unwin, London.

Howard, A. D. (1994), A detachment-limited model of drainage basin evolution, *Water Resour. Res.*, *30*, 2261–2285, doi:10.1029/94WR00757.

Huyghe, P., A. Galy, J.-L. Mugnier, and C. France-Lanord (2001), Propagation of the thrust system and erosion in the Lesser Himalaya: Geochemical and sedimentological evidence, *Geology*, *29*, 1007–1010, doi:10.1130/0091-7613(2001)029<1007:POTTSA>2.0.CO;2.

Larson, K. M., R. Buergmann, R. Bilham, and J. T. Freymueller (1999), Kinematics of the India-Eurasia collision zone from GPS measurements, *J. Geophys. Res.*, *104*, 1077–1093, doi:10.1029/1998JB900043.

Lavé, J., and J. P. Avouac (2001), Fluvial incision and tectonic uplift across the Himalayas of central Nepal, *J. Geophys. Res.*, *106*, 26,561–26,591, doi:10.1029/2001JB000359.

Meier, K., and E. Hiltner (1993), Deformation and metamorphism within the Main Central Thrust zone, Arun tectonic window, eastern Nepal, in *Himalayan Tectonics*, edited by P. J. Treolar and M. P. Searle, *Spec. Publ. Geol. Soc.*, *74*, 511–523.

Meigs, A. J., D. W. Burbank, and R. A. Beck (1995), Middle-late Miocene (>10 Ma) formation of the Main Boundary Thrust in the western Himalaya, *Geology*, *23*, 423–426, doi:10.1130/0091-7613(1995)023<0423:MLMMFO>2.3.CO;2.

Molnar, P., P. England, and J. Martinod (1993), Mantle dynamics, uplift of the Tibetan Plateau, and the Indian monsoon, *Rev. Geophys.*, *31*, 357–396, doi:10.1029/93RG02030.

Montgomery, D. R. (1994), Valley incision and the uplift of mountain peaks, *J. Geophys. Res.*, *99*, 13,913–13,921, doi:10.1029/94JB00122.

Montgomery, D. R., and D. B. Stolar (2006), Reconsidering Himalayan river anticlines, *Geomorphology*, *82*, 4–15, doi:10.1016/j.geomorph.2005.08.021.

Oberlander, T. M. (1985), Origin of drainage transverse to structures in orogens, in *Tectonic Geomorphology*, edited by M. Morisawa and J. T. Hack, pp. 155–182, Allen and Unwin, Boston.

Patriat, P., and J. Achache (1984), India-Eurasia collision chronology has implications for crustal shortening and driving mechanism of plates, *Nature*, *311*, 615–621, doi:10.1038/311615a0.

Pratt-Sitaula, B., D. W. Burbank, A. Heimsath, and T. Ojha (2004), Landscape disequilibrium on 1000–10,000 year scales Marsyandi River, Nepal, central Himalaya, *Geomorphology*, *58*, 223–241, doi:10.1016/j.geomorph.2003.07.002.

Robinson, D. M., P. G. DeCelles, P. J. Patchett, and C. N. Garzione (2001), The kinematic history of the Nepalese Himalaya interpreted from Nd isotopes, *Earth Planet. Sci. Lett.*, *192*, 507–521, doi:10.1016/S0012-821X(01)00451-4.

Robinson, D. M., P. G. DeCelles, C. N. Garzione, O. N. Pearson, T. M. Harrison, and E. J. Catlos (2003), Kinematic model for the Main Central Thrust in Nepal, *Geology*, *31*, 359–362, doi:10.1130/0091-7613(2003)031<0359:KMFTMC>2.0.CO;2.

Robinson, D. M., P. G. DeCelles, and P. Copeland (2006), Tectonic evolution of the Himalayan thrust belt in western Nepal: Implications for channel flow models, *Geol. Soc. Am. Bull.*, *118*, 865–885, doi:10.1130/B25911.1.

Sakai, H., W. Yahagi, R. Fujii, T. Hayashi, and B. N. Upreti (2006), Pleistocene rapid uplift of the Himalayan frontal ranges recorded in the Kathmandu and Siwalik basins, *Palaeogeogr. Palaeoclimatol. Palaeoecol.*, *241*, 16–27.

Schelling, D., and K. Arita (1991), Thrust tectonics, crustal shortening and the structure of the far-eastern Nepal Himalayas, *Tectonics*, *10*, 851–862, doi:10.1029/91TC01011.

Searle, M. P., R. R. Partrish, K. V. Hodges, A. Hurford, M. W. Ayres, and M. J. Whitehouse (1997), Shisha Pangma leucogranite, South Tibetan Himalayas Field relations, geochemistry, age, origin and emplacement, *J. Geol.*, *105*, 295–317.

Searle, M. P., S. R. Noble, A. J. Hurford, and D. C. Rex (1999), Age of crustal melting, emplacement and exhumation history of the Shivling Leucogranite, Garhwal Himalaya, *Geol. Mag.*, *136*, 513–525, doi:10.1017/S0016756899002885.

Seeber, L., and V. Gornitz (1983), River profiles along the Himalayan Arc as indicators of active tectonics, *Tectonophysics*, *92*, 335–367, doi:10.1016/0040-1951(83)90201-9.

Simpson, G. (2006), Influence of erosion and deposition on deformation in fold belts, *Spec. Pap. Geol. Soc. Am.*, *398*, 267–281.

Tapponier, P., and P. Molnar (1977), Active faulting and tectonics in China, *J. Geophys. Res.*, *82*, 2905–2930.

Thiede, R. C., B. Bookhagen, J. R. Arrowsmith, E. R. Sobel, and M. R. Strecker (2004), Climatic control on rapid exhumation along the Southern Himalayan Front, *Earth Planet. Sci. Lett.*, *222*, 791–806, doi:10.1016/j.epsl.2004.03.015.

Thiede, R. C., J. R. Arrowsmith, B. Bookhagen, M. O. McWilliams, E. R. Sobel, and M. R. Strecker (2005), From tectonically to erosionally controlled development of the Himalayan orogen, *Geology*, *33*, 689–692, doi:10.1130/G21483.1.

Tucker, G. E., and K. X. Whipple (2002), Topographic outcomes predicted by stream erosion models: Sensitivity analysis and intermodel comparison, *J. Geophys. Res.*, *107*(B9), 2179, doi:10.1029/2001JB000162.

Vannay, J. C., B. Grasemann, M. Rahn, W. Frank, A. Carter, V. Baudraz, and M. Cosca (2004), Miocene to Holocene exhumation of metamorphic crustal wedges in the NW Himalaya: Evidence for tectonic extrusion coupled to fluvial erosion, *Tectonics*, *23*, TC1014, doi:10.1029/2002TC001429.

Wager, L. R. (1937), The Arun drainage pattern and the rise of the Himalaya, *Geogr. J.*, *89*, 239–250.

Whipple, K. X., and G. E. Tucker (1999), Dynamics of the stream-power river incision model; implications for height limits of mountain ranges, landscape response timescales, and research needs, *J. Geophys. Res.*, *104*, 17,661–17,674, doi:10.1029/1999JB900120.

Wobus, C. W., K. V. Hodges, and K. X. Whipple (2003), Has focused denudation sustained active thrusting at the Himalayan topographic front?, *Geology*, *31*, 861–864, doi:10.1130/G19730.1.

Wobus, C. W., A. Heimsath, K. X. Whipple, and K. Hodges (2005), Active out of sequence thrust faulting in the central Nepalese Himalaya, *Nature*, *434*, 1008–1011, doi:10.1038/nature03499.

Wobus, C. W., K. X. Whipple, and K. V. Hodges (2006a), Neotectonics of the Central Nepalese Himalaya: Constraints from geomorphic, detrital $^{40}Ar/^{39}Ar$ thermochronology and thermal modelling, *Tectonics*, *25*, TC4011, doi:10.1029/2005TC001935.

Wobus, C., K. X. Whipple, E. Kirkby, N. Snyder, J. Johnson, K. Spyropolou, B. T. Crosby, and D. Sheehan (2006b), Tectonics from topography: Procedures, promise and pitfalls, *Spec Pap. Geol. Soc. Am.*, *398*, 55–74.

Yin, A., and T. M. Harrison (2000), Geologic evolution of the Himalayan-Tibetan orogen, *Annu. Rev. Earth Planet. Sci.*, *28*, 211–280, doi:10.1146/annurev.earth.28.1.211.

Zeitler, P. K., et al. (2001), Erosion, Himalayan geodynamics, and the geomorphology of metamorphism, *GSA Today*, *11*, 4–9, doi:10.1130/1052-5173(2001)011<0004:EHGATG>2.0.CO;2.

Zhang, Z., H. Wang, Z. Guo, and D. Jiang (2007), Impacts of tectonic changes on the reorganization of the Cenozoic palaeoclimatic patterns in China, *Earth Planet. Sci. Lett.*, *257*, 622–634, doi:10.1016/j.epsl.2007.03.024.

Zhao, W., K. D. Nelson, J. Che, J. Quo, D. Lu, C. Wu, and X. Liu (1993), Deep seismic reflection evidence for continental underthrusting beneath southern Tibet, *Nature*, *366*, 557–559, doi:10.1038/366557a0.

S. Hergarten, J. Robl, and K. Stüwe, Department for Earth Sciences, University of Graz, Heinrichstr. 26, A-8010 Graz, Austria. (joerg.robl@uni-graz.at)